ACS NANO
Cite This: *ACS Nano* 2018, 12, 1120−1127
www.acsnano.org

ARTICLE

Large Enhancement of Thermal Conductivity and Lorenz Number in Topological Insulator Thin Films

Zhe Luo,[†,#] Jifa Tian,[‡,#] Shouyuan Huang,[†,#] Mithun Srinivasan,[†] Jesse Maassen,[*,§] Yong P. Chen,[*,‡,∥] and Xianfan Xu[*,†,∥]

[†]School of Mechanical Engineering and Birck Nanotechnology Center, [‡]Department of Physics & Astronomy and Birck Nanotechnology Center, and [∥]School of Electrical and Computer Engineering, Purdue University, West Lafayette, Indiana 47907, United States

[§]Department of Physics and Atmospheric Science, Dalhousie University, Halifax, Nova Scotia B3H 4R2, Canada

Supporting Information

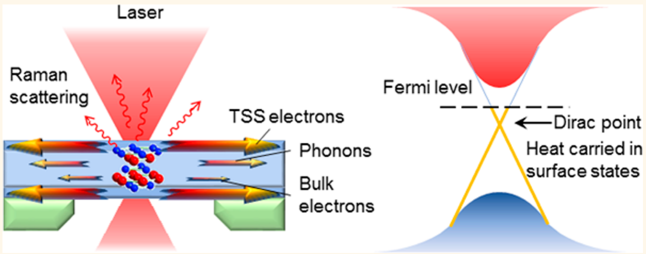

ABSTRACT: **Topological insulators (TI) have attracted extensive research effort due to their insulating bulk states but conducting surface states. However, investigation and understanding of thermal transport in topological insulators, particularly the effect of surface states, are lacking. In this work, we studied thickness-dependent in-plane thermal and electrical conductivity of Bi_2Te_2Se TI thin films. A large enhancement in both thermal and electrical conductivity was observed for films with thicknesses below 20 nm, which is attributed to the surface states and bulk-insulating nature of these films. Moreover, a surface Lorenz number much larger than the Sommerfeld value was found. Systematic transport measurements indicated that the Fermi surface is located near the charge neutrality point (CNP) when the film thickness is below 20 nm. Possible reasons for the large Lorenz number include electrical and thermal current decoupling in the surface state Dirac fluid, and bipolar diffusion transport. A simple computational model indicates that the surface states and bipolar diffusion indeed can lead to enhanced electrical and thermal transport and a large Lorenz number.**

KEYWORDS: *topological insulator, thermal conductivity, Lorenz number, electrical conductivity, Dirac fluid*

A three-dimensional (3D) topological insulator (TI) has a bulk band gap and behaves as an insulator in its interior but possesses protected conducting electronic states on its surface known as topological surface states (TSS).[1−3] With the spin texture and linear energy-momentum dispersion of the TSS, TIs exhibit exotic quantum-physical properties and have been extensively studied for the past decade.[4−9] From a practical perspective, the spin-momentum locking of TSS may yield a dissipationless spin current at the TI surface, which is of great potential in applications such as spintronics and quantum computation.[1,2] Despite the abundant research efforts regarding TIs, studies regarding thermal transport in TSS are rare. In usual 3D semiconductor solids, thermal energy is transferred through bulk electrons (or holes) and phonons. For TIs, TSS provide yet another possible heat conducting channel involving Dirac electrons, which may give rise to intriguing heat-transfer phenomena. Among the TI materials, Bi_2Te_2Se (BTS221) has been shown to have a minimal bulk contribution to electronic transport and prominent TSS properties,[10−12] which serves as a good platform to study thermal transport arising from TSS carriers. In the past the Bi−Te−Se family material has been investigated as thermoelectric materials.[13−16] It has also been proposed that TIs can exhibit large thermoelectric figure-of-merit enhancement by proper manipulations of TSS,[17−20] which brings more interest to the investigation of thermal transport of TI surface states.

Here, we report studies of in-plane thermal conductivity of BTS221 TI films using Raman thermometry,[21−26] together with detailed transport measurements of electrical conductivity. Raman thermometry is a well-established technique that utilizes laser heating and measures the resulting temperature rise from Raman scattering spectra and then extracts thermal transport properties from temperature data. Our results and analysis show that both effective 3D electrical and thermal conductivity increase significantly as the BTS221 film thickness decreases, which accounts for ~70% of the electrical conductance and nearly half of the total thermal conductance when the thickness

Received: September 9, 2017
Accepted: January 23, 2018
Published: January 23, 2018

DOI: 10.1021/acsnano.7b06430
ACS Nano 2018, 12, 1120−1127

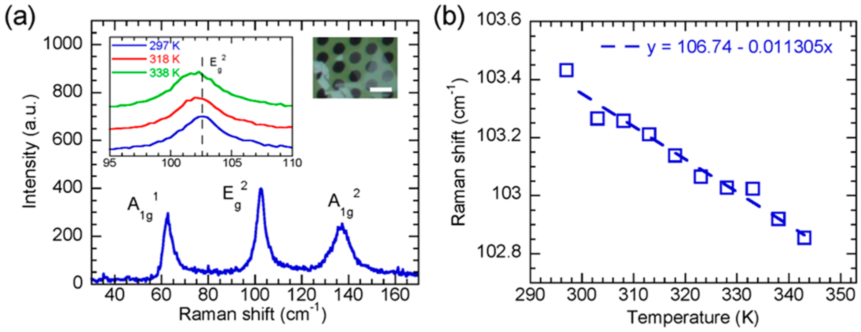

Figure 1. Raman thermometer calibration of a 10 nm thick BTS221 film. (a) Raman spectrum of the film. Left inset: Typical Raman spectra of the E_g^2 mode at various temperatures. Right inset: Optical image of the transferred film, scale bar: 5 μm. (b) E_g^2 mode Raman shift *vs* temperature. Dashed line is linear fit, whose slope is the temperature coefficient.

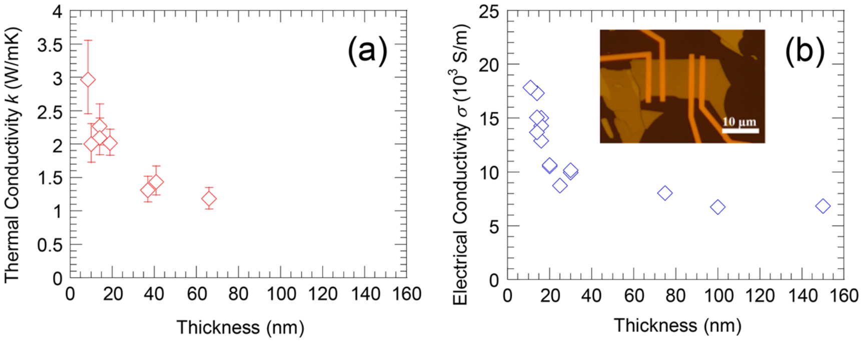

Figure 2. Thermal and electrical transport of BTS221 thin films. (a) Thickness dependence of the effective in-plane thermal conductivity k measured by the Raman thermometry. (b) Effective 3D electrical conductivity σ at V_g = 0 V. Relative uncertainty of data is ±2.5%. All measurements are made at room temperature. Inset: optical graph of a typical device.

is below 20 nm. The measured low carrier density and the observed ambipolar field effect in the thin samples confirm their topological nature. An exceptionally large Lorenz number compared to the Sommerfeld value is found, demonstrating the surface states provide additional thermal transport channels in BTS thin films. Possible reasons for the large Lorenz number include electrical and thermal current decoupling in the surface state Dirac fluid and the bipolar diffusion transport. A simple computational model indicates that the surface states and bipolar diffusion indeed can lead to enhanced electrical and thermal transport and large Lorenz number.

RESULTS AND DISCUSSION

BTS221 thin films were prepared via tape exfoliation from bulk crystals synthesized by the Bridgman technique. Both the ARPES and transport results demonstrate that our bulk crystals possess clear TSS which may have significant contribution on the transport even at room temperature.[27] The exfoliated thin films were subsequently suspended on holey SiN membranes using a wet transfer technique for Raman thermometry measurements (see the Experimental Methods and previous work[25,26]). To unveil the role of surface states in the overall thermal transport in BTS221, extensive effort was put forward to bring the thickness down to 8 nm in order to reduce the bulk contribution as much as possible. Figure 1a shows Raman spectra and an optical image of a suspended 10 nm flake at elevated temperature. The E_g^2 mode was used as the Raman thermometer for its good sensitivity to temperature change, with a temperature coefficient $\chi_{Eg2} = -0.0113$ cm^{-1}/K where $\chi = \Delta\omega/\Delta T$, with ω being the frequency and T the temperature (Figure 1b).

In the Raman thermometry measurements, the suspended BTS221 films were heated by a He−Ne laser at various powers. The temperature rise from laser heating was determined by the shift in the E_g^2 Raman peak and subsequently used in a 2D numerical heat-transfer model to extract the in-plane thermal conductivity (see Experimental Methods and ref 26 for details). The measurements were carried out near room temperature (300 K), and the results are shown in Figure 2a. As the thicknesses of the BTS221 films decrease to less than 20 nm, the measured effective in-plane thermal conductivity k undergoes a rapid increase from ∼1 to ∼3 W/mK for films less than 10 nm thick, indicating the possible contributions from surface carriers (the uncertainty analyses are provided in the Supporting Information). Meanwhile, electrical-transport measurements were conducted on a number of BTS221 devices with different thicknesses. For these electrical transport measurements, BTS221 flakes were exfoliated on a Si wafer with 300 nm thermally grown SiO_2 on top. Four Cr/Au electrodes were patterned using electron beam lithography (EBL) and standard lift-off processes, and four-probe sheet resistance R_S measurements were carried out at V_g = 0 V. Figure 2b shows the thickness-dependent effective 3D electrical conductivity $\sigma = 1/(R_S t)$ measured at room temperature where t is the film thickness. As seen in Figure 2b, σ also has an uprising trend when the thickness is less than ∼20 nm, similar to the thermal conductivity data in Figure 2a.

The higher effective 3D electrical conductivity at smaller thicknesses in BTS221 films can be attributed to the increase of TSS contribution due to the reduced bulk conduction.[10] Generally in TIs, the topological surface state gives a metallic conducting layer at the surface of the TI, while the bulk interior

DOI: 10.1021/acsnano.7b06430
ACS Nano 2018, 12, 1120−1127

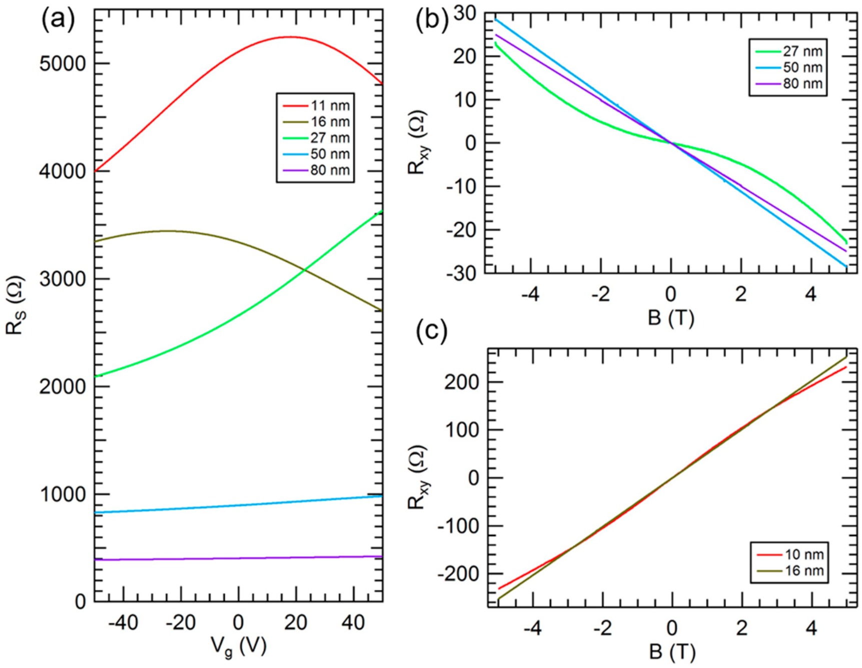

Figure 3. Field and Hall effects of BTS221 thin films. (a) Sheet resistance as a function of back gate voltage (V_g) measured on samples with different thicknesses. (b, c) Corresponding Hall effects of the samples at V_g = 0 V. All of the measurements were performed at room temperature.

can be much less conducting if its carrier density (doping) is low. Furthermore, the surface state electrons can have high mobility[10,27] (~2000 cm^2/(V s) at low T and ~500 cm^2/(V s) at room T for our samples) and weak electron−phonon coupling with the insulating bulk.[28,29]

To confirm the contribution of TSS to electrical conduction in the thin samples, we have systematically studied the electrical field and Hall effects of the BTS221 samples (Figure 3 and Supplementary Figures 7 and 8) at various thicknesses. Figure 3 represents the corresponding sheet resistance R_s as a function of back gate voltage (V_g) and Hall resistance (R_{xy}) as a function of magnetic field (B) measured at room temperature. We see that the sample sheet resistance (or the carrier density) of all samples can be modulated by back gating, and a clear ambipolar field effect is observed when the thickness is below 20 nm. This conclusion is further supported by the corresponding Hall effect measured at V_g = 0 V (Figure 3b,c). For thick BTS221 samples (>30 nm), the curves of Hall resistance *vs* B field are linear and have a small Hall coefficient (R_H) (Figure 3b). The 2D carrier density extracted from R_H using a single-band model is on the order of 10^{14} cm^{-2}, demonstrating that the electrical transport is dominated by bulk (hole) carriers. When the sample thickness is below 20 nm, R_H changes sign (Figures 3b,c), which is consistent with the observed ambipolar field effect (Figure 3a), indicating the carrier type changes from hole to electron as the thickness decreases. The extracted 2D carrier densities from R_H (by using $R_H = 1/ne$) of the thin samples are ~1.0 × 10^{13} cm^{-2} (thus, 5 × 10^{12} cm^{-2} for one surface), which is ~10 times smaller than that of the thick sample (Figure 3b). From the ARPES results of BTS221 bulk crystals,[23] we know that when the Fermi level is located at the bottom of conduction band, the carrier density on one surface is ~1.0 × 10^{13} cm^{-2}, which is two times higher than the carrier density (5 × 10^{12} cm^{-2} for one surface) extracted from our thin samples. Therefore, the transport in our thin samples with a low carrier density are contributed more by the TSS. We further find that the room-temperature 2D carrier density (~1.2 × 10^{13} cm^{-2}) of the 18 nm flake is only ~1.7 times higher than that measured at T = 1.6 K (~7.0 × 10^{12} cm^{-2}), whereas it is 5 times higher for a 50 nm thick sample (Supplementary Figure 8). We further note that the Hall resistance of our thin samples shows nonlinearity (Figure 3b). Thus, the actual carrier density is expected to be even lower than the "single-band" carrier density extracted from the nonlinear Hall resistance. We further rule out the possible contribution from the band-bending induced trivial surface states since they are derived from the bulk states and far away for the CNP (if such states were populated we would expect to have a much higher carrier density exceeding ~1.0 × 10^{13} cm^{-2} per surface).

To further quantify the contribution of surface states to electrical and thermal transport, we analyze the electrical conductivity and thermal conductivity data using a two-layer transport model accounting for the contributions from surface states and bulk. The total electrical conductance (G) and thermal conductance (Γ) are approximated as

$$G = G_{\text{surf}} + G_{\text{bulk}} = G_{\text{surf}} + \sigma_{\text{bulk}} t \quad (1a)$$

$$\Gamma = \Gamma_{\text{surf}} + \Gamma_{\text{bulk}} = \Gamma_{\text{surf}} + k_{\text{bulk}} t \quad (1b)$$

The subscripts "surf" and "bulk" represent contributions from surface and bulk, respectively. $G = \sigma t$ and $\Gamma = kt$ are the conductance for the entire film. Here underlies an assumption that the bulk thermal conductivity k_{bulk} is independent of the thickness, which does not hold if the thickness is smaller than the phonon mean-free-path. It is noted for a similar material, Bi_2Te_3, that more than 80% of heat is carried by phonons with a phonon mean free path shorter than 8 nm.[15] As our films have thicknesses larger than 8 nm, it is expected the reduction of bulk thermal conductivity due to boundary scattering is small. However, if the reduction of bulk thermal conductivity due to a smaller mean-free-path in thin films is considered, an even higher surface contribution to the total thermal conductance

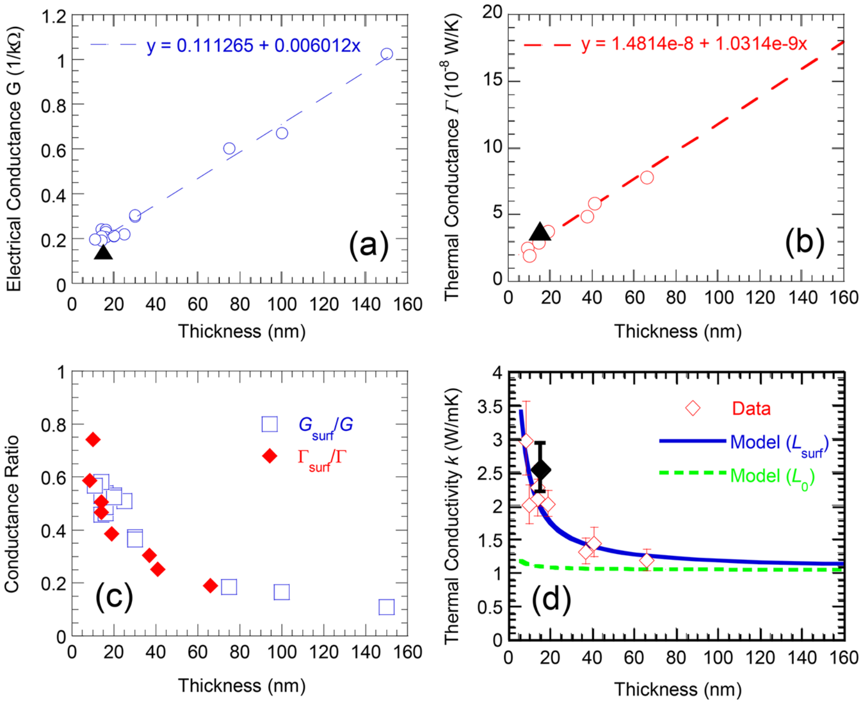

Figure 4. Analyses of the transport properties of BTS221 thin films to extract surface and bulk contributions. (a) Electrical sheet conductance G_{tot} measured at V_g = 0 V and a linear fit (dashed line). (b) Thermal conductance Γ and linear fit. (c) Calculated ratio of surface electrical (thermal) conductance G_{surf} (Γ_{surf}) to the total conductance G (Γ). (d) Fitting the in-plane thermal conductivity k (experimental data from Figure 2a) using the extracted Lorenz number L and Sommerfeld value L_0 in eq 2. The black pyramid symbol in (a) and (b), and the black diamond in (d) represents the value obtained from a separate four-terminal BTS221−SiN device.

will be obtained, which will be consistent with our main conclusions discussed below. An analysis of the effect of the reduction of bulk thermal (and electrical) conductivity is provided in the Supporting Information, which shows that the surface contribution is indeed larger when the surface scattering is considered.

The thickness-dependent total electrical and thermal conductance calculated ($G_s = \sigma t$, $\Gamma_s = kt$) from the experimental data (σ and k) are shown in Figure 4a,b. The linear fit of both data show a non-zero intercept, which is attributed to the surface conductance, and the slope is the bulk conductivity: G_{surf} = 0.11 kΩ^{-1}, σ_{bulk} = 6.0 × 10^3 S/m, Γ_{surf} = 1.4 × 10^{-8} W/K, and k_{bulk} = 1.0 W/mK. Figure 4c shows the surface electrical (thermal) conductance to the total electrical (thermal) conductance ratio, G_{surf}/G (Γ_{surf}/Γ). As the thickness decreases, the contribution from the surface conductance rises up from less than 20% up to 60% for electrical conductance, and up to 70% for thermal conductance. The extracted room-temperature bulk electrical resistivity $\rho = 1/\sigma \sim 0.017$ Ω·cm, is comparable with the reported resistivity 0.01−0.02 Ω·cm measured in thicker BTS221 bulk crystals.[10] The bulk thermal conductivity value is also consistent with previously reported theoretical and experimental data of Bi_2Te_3,[13,16,30] which is of similar lattice structure as BTS221. The results show that, at sufficiently small thickness, the electrical and thermal transport of thin BTS221 film are significantly influenced by the surface state, consistent with our field and Hall effects (Figure 3 and Supplementary Figures 7 and 8).

The relation between the thermal and electrical conductivity is described by the Wiedemann−Franz law, $k_e/\sigma = LT$, where k_e is thermal conductivity due to charge carriers and L is the Lorenz number. Rewriting it in conductance form gives $\Gamma/G = LT$. For the surface contribution in the measured BTS221 thin films, a surface Lorenz number L_{surf} is defined here as $\Gamma_{surf}/G_{surf} = L_{surf}T$. G_{surf} and Γ_{surf} are the surface electrical and thermal conductance from fitting parts a and b, respectively, of Figure 4, respectively. This gives us an estimation of the surface Lorenz number. It is found that L_{surf} = (4.2 ± 0.8) × 10^{-7} V^2/K^2, over 10 times larger than the Sommerfeld value L_0 = 2.44 × 10^{-8} V^2/K^2, the theoretical value for metals and highly degenerate semiconductors.

To compare the experimentally measured total thermal conductivity with the model prediction using either L_{surf} or L_0, the in-plane thermal conductivity is calculated using the following equation following eq 2:

$$k = \frac{\Gamma_{surf}}{t} + k_{bulk} = \frac{LTG_{surf}}{t} + k_{bulk} \tag{2}$$

We use both L_{surf} and the Sommerfeld value L_0 in the calculation, and the calculated k values (using eq 2, with G_{surf} and k_{bulk} fitted above) are shown as solid and dashed lines in Figure 4d. The line calculated using L_{surf} fits the experimental data reasonably well, while the line using L_0 cannot capture the significant thermal conductivity rise for thinner films. Note that we are not able to separate the contributions of bulk electrons and phonons in Γ, so the Lorenz number L_{bulk} for bulk electrons cannot be extracted.

An alternative way to estimate the Lorenz number without using the linear extrapolation is directly using the measured data for the thinnest films studied. We assume that for the measured thermal conductivity, the phonon contribution is 1 W/mK, the value we measured for thicker films, and subtract this value from the measured thermal conductivity to obtain the thermal conductivity from charge carriers, k_e. This will give us a lower bound of the Lorenz number since the phonon contribution is likely to be less for thin films. For the 8 nm-

DOI: 10.1021/acsnano.7b06430
ACS Nano 2018, 12, 1120−1127

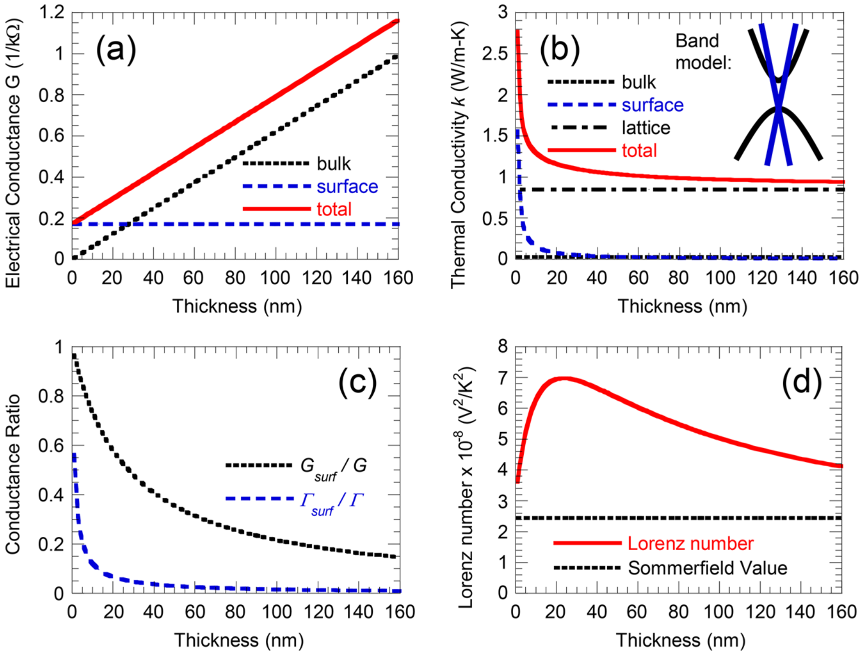

Figure 5. Calculated transport properties of BTS221 thin films with surface and bulk contributions. (a) Electrical sheet conductance G *versus* film thickness, with contributions from surface and bulk. (b) Thermal conductivity k *versus* film thickness, with contributions from surface, bulk, and lattice. (c) Ratio of surface electrical (thermal) conductance G_{surf} (Γ_{surf}) to the total conductance G(Γ). (d) Lorenz number versus film thickness, compared against the Sommerfeld value 2.44×10^{-8} V^2/K^2.

thick film, its k_e and G values are 1.96 W/mK and 0.16 1/kΩ. This yields a total Lorenz number of 3.2×10^{-7} V^2/K^2, including effects from both surface and bulk electrons, which is also significantly higher than the Sommerfeld value.

There was a concern that the SiO_2 dielectric layer underneath the TI film used for the electrical measurements could alter the electronic properties of the TI films to be different from those suspended TI films (without such a SiO_2 substrate layer) in the thermal transport measurements, for example by shifting the Fermi level relative to the Dirac point.[31,32] There was also a concern that the BTS221 device fabrication process for the electrical measurements could alter the quality of the BTS221 films. To check this, a four-probe device was first patterned on SiN membrane, and then the BTS221 flake was transferred onto the probes. The same sample was then used for both thermal and electrical conductivity measurements at room temperature. Therefore, this flake did not go through any nanofabrication processes. The measurement results are shown as the black pyramid symbol in Figure 4a,b,d. It is seen that the measured electrical conductance and thermal conductivity are in good agreement with other experimental data, and they also lie in vicinity of the model prediction using the large L_{surf}.

Now we discuss the possible reasons for the large surface Lorenz number or the large Lorenz number for very thin films. The observed large surface Lorenz number L_{surf} can be attributed to several possible origins. One possible reason for the observed large Lorenz number is the bipolar diffusion in semiconductor materials.[33] Wiedemann–Franz law is based on the single band picture, so that when two or more bands contribute to transport, Wiedemann–Franz law can break down.[34] When both electrons and holes are thermally excited (for example, in nondegenerate semiconductors with small band gap at room or elevated temperature) and a temperature difference is created, the carriers diffuse to the colder region. In addition to the sum of the thermal transport by electrons and holes separately, the carrier recombination at the colder side releases energy, which enhances the total thermal conductivity.[13,35] This can be the case for the zero band gap, nearly charge neutral surface states as the electrons and holes are readily excited thermally. Based on the Boltzmann transport equation, the electronic thermal conductivity k_e can be written as[33]

$$k_e = k_n + k_p + \frac{\sigma_n \sigma_p}{\sigma_n + \sigma_p}(\alpha_n + \alpha_p)^2 T \tag{3}$$

where α is the Seebeck coefficient. The third term comes from the bipolar diffusion which takes a maximum value when $\sigma_n = \sigma_p$, and it could be much larger than either k_n and k_p. Therefore, the bipolar contribution is in favor of small band gap (for high σ_n and σ_p) as well as the Fermi level pinned around the neutrality point to achieve $\sigma_n = \sigma_p$. While enhancing heat transfer, bipolar diffusion does not increase electrical conductivity (meaning $\sigma = \sigma_n + \sigma_p$), hence resulting in an increased Lorenz number. Experimentally, bipolar effect enhanced electronic thermal conductivity was previously observed at elevated temperature in small-gap semiconductors such as Bi_2Te_3,[13] Al-based quasicrystals,[36] and $In_4Se_{3-x}Te_x$.[37] Further, first-principles calculations predict that a large increase of Lorenz number (up to 10 times the Sommerfeld value) can occur in Bi_2Te_3[16,38] and skutterudites[39] when the Fermi level sits near the charge neutral point (center of the bulk band gap). Additionally, it has been predicted that the bipolar effect exists for Dirac electrons in graphene with a 1.8- to 4-fold increase of L at room temperature, or any systems with a zero band gap and near charge neutrality condition.[35] Our BTS221 thin films do have a small bulk band gap measured to be ~0.3 eV[27] and gapless TSS. Moreover, as discussed above, transport measurements indeed indicated that for thicknesses less than 20 nm, our samples were nearly charge neutral. Therefore, in our case, it is possible that the thermally populated surface electrons and holes are involved in the bipolar diffusion process that causes the observed large Lorenz number in our BTS221 thin films. We note that another possible cause for the large Lorenz number in our TI samples is the band bending induced trivial surface states.[27] However, as discussed earlier, we have ruled out such a contribution because the Fermi levels of our thin samples are located in TSS and close to the CNP.

Another possibility is the effect of Dirac fluid of TSS electrons, with a strongly interacting electron−hole plasma formed near the Dirac point.[40,41] The Dirac fluid theory suggests that when the electron−electron scattering is the dominating charge carrier scattering mechanism, the hydrodynamic nature of the charge carriers leads to the decoupling of charge and (electronic) heat current.[40−42] In this case, the charge current is limited by the viscosity of Dirac fluid, while the heat current carried by electrons (holes) is limited only by impurity scattering. This will inevitably lead to the breakdown of the Wiedemann−Franz law, which has been theoretically predicted in graphene.[43,44] Indeed, a nearly 20-fold increase of the Lorenz number over the Sommerfeld value was recently experimentally observed in graphene near 75 K.[40] In our case, as the sample thickness decreases from 80 nm to below 20 nm, the extracted carrier density decreases by more than 1 order of magnitude and the transport in our thin samples is dominated by the TSS with its Fermi level near the CNP (Figure 3). Furthermore, the observed nonlinearity of the Hall resistance in the samples indicates the coexistence of electrons and holes (Figure 3). Thus, in our thin samples, the majority of electrical and/or thermal transport originates from both the electrons and holes near the CNP of TSS, where the coupling between electronic and heat currents due to the charge carrier (electron or hole) may be significantly weakened, which can lead to a large Lorenz number.

To illustrate the possible contributions from surface states and bipolar diffusion to the transport processes, we utilize a simple electronic band model to calculate the transport properties and provide some physical insight. Our adopted band model for BTS221, depicted in the inset of Figure 5b, includes a 3D parabolic dispersion ($E(k) = \hbar^2 k_{3D}^2/2m^*$) for the conduction and valence bands (bulk states) and a 2D linear dispersion ($E(k) = \hbar v_F k_{2D}$) for the TSS band (surface states). The bulk bands are 3D, the number of states increases with film thickness, whereas the 2D surface bands have a constant number of states. Using this simple electronic band model, and assuming a constant mean-free-path for the surface and bulk states, we solve the Boltzmann transport equation within the Landauer approach[45,46] and extract the electronic conductivity, Seebeck coefficient, electronic thermal conductivity, and Lorenz number. Note that bipolar, or multiband, effects are included in the calculation. Details of the modeling parameters and calculation method are provided in the Supporting Information. Figure 5a shows the calculated electrical sheet conductance (electrical conductivity times film thickness) versus film thickness. The total G scales linearly with thickness, as a thicker film increases the number of conducting bulk states. As the film thickness goes to zero, a constant contribution from the surface states remains. The thermal conductivity, presented in Figure 5b, increases with decreasing film thickness, as the surface contribution becomes larger and dominates in the thinnest films. With thicker films the lattice contribution is dominant (the phonon contribution is approximately 0.85 W/mK, see the Supporting Information). To illustrate the contribution of the surface states to the electrical and heat transport characteristics, Figure 5c shows the calculated G_{surf}/G and Γ_{surf}/Γ. As expected the surface states play an important role in the thinnest films, when there are fewer bulk conduction channels. Γ_{surf}/Γ is smaller than G_{surf}/G in part because of the lattice contribution to thermal conductivity which increases Γ. The calculated Lorenz number, presented in Figure 5d, is found to be greater than the Sommerfeld value and shows a peak value of 7×10^{-8} V^2/K^2 for a 20 nm thickness. L is thickness dependent due to the relative contributions of surface versus bulk (including the bipolar diffusion) conduction, and exhibits a peak when both are roughly equal. The calculation also shows that the maximum L from the surface states alone is 5.8×10^{-8} V^2/K^2, and the combination of both surface and bulk leads to an effective L that is greater than their individual components. This simple band model shows results consistent with experimentally observed trends and demonstrates a large contribution to transport from the surface states in the thinnest films. Differences between theory and experiment can result from the band model and the parameters used, for example, a thickness dependence of the Fermi level in the samples and the particular energy dependence of the dominant scattering mechanism and the mean-free-paths.

CONCLUSIONS

The thickness-dependent in-plane thermal and electrical conductivity of BTS221 TI thin films was studied and a large enhancement was observed when the thickness is reduced to less than 20 nm. Moreover, a Lorenz number much larger than the Sommerfeld value for the TI surface was found. Possible mechanisms include the transport properties of surface states due to the electrical and thermal current decoupling in the Dirac fluid as well as bipolar diffusion of electrons and holes at TI surface. A simple computational model was employed to explain that the surface states and bipolar diffusion can indeed lead to enhanced electrical and thermal transport and large Lorenz number. Further work is needed to examine the detailed relative importance of these two mechanisms (or possible involvement of additional mechanisms) in the observed enhancement of the Lorenz number.

EXPERIMENTAL METHODS

Sample Preparation. BTS221 flakes were exfoliated using dicing tape onto poly(methyl methacrylate) (PMMA) and poly(vinyl alcohol) (PVA) thin film stack spin-coated onto Si wafer. The film stack with flakes was examined under the microscope to identify candidate flakes for transfer, then the desired flakes were precisely aligned to the holey silicon nitride membrane (Ted Pella) and attached. The entire sample was then soaked into acetone to remove the PMMA, leaving the flakes suspended on the holes for Raman thermal measurements. The thin films were suspended on through-holes, which avoids additional laser absorption during Raman thermometry experiments. For electrical measurements, BTS221 flakes (typical thickness ∼10−200 nm) are tape-exfoliated and placed on top of heavily doped Si substrates capped with 300 nm SiO_2. TI flakes with different thicknesses are selected under the optical microscope and characterized using atomic force microscopy (AFM). The four-terminal (inset of Figure 2b) and Hall bar electrodes (Supplementary Figure 6) of the devices are fabricated by e-beam lithography, followed by e-beam deposition of Au/Cr (90/5 nm). The sample resistances R are measured using the standard 4-terminal lock-in technique with an AC driving current of 1 μA at 13.33 Hz. The sample sheet resistance R_S is calculated by $R_S = R \times W/L$, where W and L are the width and length of the conduction channel in the TI device, respectively. All the electrical conductivity measurements are performed at room temperature and ambient pressure. The field and Hall effects are performed at both room and low temperatures in a variable temperature insert system with a base temperature of 1.6 K.

Raman Thermometry Measurements. A HORIBA LabRAM HR800 system was used. A 632.8 nm wavelength He−Ne laser focused by a 100x (Olympus MPLN 100x, NA(dry) = 0.90) objective was used both as a heat source and Raman excitation source. The grating used has a groove density of 1800 l/mm, which gives a nominal spectral resolution of 0.27 cm^{-1} per pixel. The Raman spectra were fitted using Lorentzian function to extract the Raman peak position, and the Lorentzian peak fitting yields a peak position shift uncertainty less than 0.02 cm^{-1}, corresponding to a temperature rise measurement uncertainty of 1 K. The reflectivity of each suspended film was measured by the same laser using a silver-coated mirror as reference with known reflectivity, while the transmissivity of the sample was obtained by a photon detector placed underneath it. Then the amount of absorbed laser power was derived from the reflectivity, transmissivity and the total incident laser power, and was subsequently used as heat source input for the numerical heat transfer model to extract the in-plane thermal conductivity of the suspended thin film. More details can be found in the Supporting Information.

ASSOCIATED CONTENT

Supporting Information

The Supporting Information is available free of charge on the ACS Publications website at DOI: 10.1021/acsnano.7b06430.

> Raman thermometry, uncertainty of the thermal conductivity measurement and the calculated surface Lorentz number, surface and bulk carriers' contribution considering surface scattering, thermal expansion effects in Raman measurements and slip test, suspended four-terminal BTS221 device for validation purpose and typical Hall bar device, additional transport evidence to confirm the significant contributions from TSS in our thin samples, and theoretical model and approach for calculating transport properties (PDF)

AUTHOR INFORMATION

Corresponding Authors

*Email: jmaassen@dal.ca.
*Email: yongchen@purdue.edu.
*Email: xxu@ecn.purdue.edu.

ORCID

Jifa Tian: 0000-0003-2921-470X
Xianfan Xu: 0000-0003-0580-4625

Author Contributions

[#]Z.L., J.T., and S.H. contributed equally to this work.

Author Contributions

X.X. and Y.P.C. conceived the idea and supervised the experiments. Z.L. led the thermal conductivity experiments, Z.L., S.H., and M.S. performed the thermal conductivity measurements, and Z.L. and S.H. analyzed the thermal conductivity data. J.T. performed and analyzed the electrical transport measurements. J.M. performed transport calculations. All authors cowrote the manuscript.

Notes

The authors declare no competing financial interest.

ACKNOWLEDGMENTS

This work was partly supported by DARPA MESO (Grant No. N66001-11-1-4107) and NSF (EFMA-1641101). J.M. acknowledges support from NSERC (Discovery Grant RGPIN-2016-04881). We also thank J. Heremans for valuable discussions.

REFERENCES

(1) Moore, J. E. The Birth of Topological Insulators. *Nature* **2010**, *464*, 194−198.

(2) Hasan, M. Z.; Kane, C. L. Colloquium: Topological Insulators. *Rev. Mod. Phys.* **2010**, *82*, 3045−3067.

(3) Ando, Y. Topological Insulator Materials. *J. Phys. Soc. Jpn.* **2013**, *82*, 102001.

(4) Bernevig, B. A.; Hughes, T. L.; Zhang, S.-C. Quantum Spin Hall Effect and Topological Phase Transition in HgTe Quantum Wells. *Science* **2006**, *314*, 1757−1761.

(5) Hsieh, D.; Xia, Y.; Qian, D.; Wray, L.; Dil, J. H.; Meier, F.; Osterwalder, J.; Patthey, L.; Checkelsky, J. G.; Ong, N. P.; Fedorov, A. V.; Lin, H.; Bansil, A.; Grauer, D.; Hor, Y. S.; Cava, R. J.; Hasan, M. A. A Tunable Topological Insulator in the Spin Helical Dirac Transport Regime. *Nature* **2009**, *460*, 1101−1105.

(6) Qi, X.-L.; Zhang, S.-C. The Quantum Spin Hall Effect and Topological Insulators. *Phys. Today* **2010**, *63*, 33.

(7) Chang, C.-Z.; Zhang, J.; Feng, X.; Shen, J.; Zhang, Z.; Guo, M.; Li, K.; Ou, Y.; Wei, P.; Wang, L.-L.; Ji, Z.-Q.; Feng, Y.; Ji, S.; Chen, X.; Jia, J.; Dai, X.; Fang, Z.; Zhang, S.-C.; He, K.; Wang, Y.; et al. Experimental Observation of the Quantum Anomalous Hall Effect in a Magnetic Topological Insulator. *Science* **2013**, *340*, 167−170.

(8) Xu, Y.; Miotkowski, I.; Liu, C.; Tian, J.; Nam, H.; Alidoust, N.; Hu, J.; Shih, C.-K.; Hasan, M. Z.; Chen, Y. P. Observation of Topological Surface State Quantum Hall Effect in an Intrinsic Three-Dimensional Topological Insulator. *Nat. Phys.* **2014**, *10*, 956−963.

(9) Jauregui, L. A.; Pettes, M. T.; Rokhinson, L. P.; Shi, L.; Chen, Y. P. Magnetic Field Induced Helical Mode and Topological Transitions in a Quasi-Ballistic Topological Insulator Nanoribbon with Circumferentially Quantized Surface State Sub-Bands. *Nat. Nanotechnol.* **2016**, *11*, 345−351.

(10) Ren, Z.; Taskin, A. A.; Sasaki, S.; Segawa, K.; Ando, Y. Large Bulk Resistivity and Surface Quantum Oscillations in the Topological Insulator Bi_2Te_2Se. *Phys. Rev. B: Condens. Matter Mater. Phys.* **2010**, *82*, 241306.

(11) Taskin, A. A.; Ren, Z.; Sasaki, S.; Segawa, K.; Ando, Y. Observation of Dirac Holes and Electrons in a Topological Insulator. *Phys. Rev. Lett.* **2011**, *107*, 16801.

(12) Xiong, J.; Luo, Y.; Khoo, Y.; Jia, S.; Cava, R. J.; Ong, N. P. High-Field Shubnikov-de Haas Oscillations in the Topological Insulator Bi_2Te_2Se. *Phys. Rev. B: Condens. Matter Mater. Phys.* **2012**, *86*, 45314.

(13) Goldsmid, H. The Thermal Conductivity of Bismuth Telluride. *Proc. Phys. Soc., London, Sect. B* **1956**, *69*, 203−209.

(14) Scherrer, S.; Scherrer, H. Thermoelectric Properties of Bismuth Antimony Telluride Solid Solutions. In *Thermoelectrics Handbook*; CRC Press, 2005; pp 19−27.

(15) Wang, Y.; Qiu, B.; McGaughey, A. J. H.; Ruan, X.; Xu, X. Mode-Wise Thermal Conductivity of Bismuth Telluride. *J. Heat Transfer* **2013**, *135*, 91102.

(16) Pettes, M. T.; Maassen, J.; Jo, I.; Lundstrom, M. S.; Shi, L. Effects of Surface Band Bending and Scattering on Thermoelectric Transport in Suspended Bismuth Telluride Nanoplates. *Nano Lett.* **2013**, *13*, 5316−5322.

(17) Ghaemi, P.; Mong, R. S. K.; Moore, J. E. In-Plane Transport and Enhanced Thermoelectric Performance in Thin Films of the Topological Insulators Bi_2Te_3 and Bi_2Se_3. *Phys. Rev. Lett.* **2010**, *105*, 166603.

(18) Luo, X.; Sullivan, M. B.; Quek, S. Y. First-Principles Investigations of the Atomic, Electronic, and Thermoelectric Properties of Equilibrium and Strained Bi_2Se_3 and Bi_2Te_3 Including van Der Waals Interactions. *Phys. Rev. B: Condens. Matter Mater. Phys.* **2012**, *86*, 184111.

(19) Xu, Y.; Gan, Z.; Zhang, S.-C. Enhanced Thermoelectric Performance and Anomalous Seebeck Effects in Topological Insulators. *Phys. Rev. Lett.* **2014**, *112*, 226801.

(20) Rittweger, F.; Hinsche, N. F.; Zahn, P.; Mertig, I. Signature of the Topological Surface State in the Thermoelectric Properties of Bi_2Te_3. *Phys. Rev. B: Condens. Matter Mater. Phys.* **2014**, *89*, 35439.

(21) Cai, W.; Moore, A. L.; Zhu, Y.; Li, X.; Chen, S.; Shi, L.; Ruoff, R. S. Thermal Transport in Suspended and Supported Monolayer Graphene Grown by Chemical Vapor Deposition. *Nano Lett.* **2010**, *10*, 1645−1651.

(22) Yan, R.; Simpson, J. R.; Bertolazzi, S.; Brivio, J.; Watson, M.; Wu, X.; Kis, A.; Luo, T.; Walker, A. R. H.; Xing, H. G. Thermal Conductivity of Monolayer Molybdenum Disulfide Obtained from Temperature-Dependent Raman Spectroscopy. *ACS Nano* **2014**, *8*, 986−993.

(23) Zhou, H.; Zhu, J.; Liu, Z.; Yan, Z.; Fan, X.; Lin, J.; Wang, G.; Yan, Q.; Yu, T.; Ajayan, P. M.; Tour, J. M. High Thermal Conductivity of Suspended Few-Layer Hexagonal Boron Nitride Sheets. *Nano Res.* **2014**, *7*, 1232−1240.

(24) Peimyoo, N.; Shang, J.; Yang, W.; Wang, Y.; Cong, C.; Yu, T. Thermal Conductivity Determination of Suspended Mono- and Bilayer WS_2 by Raman Spectroscopy. *Nano Res.* **2015**, *8*, 1210−1221.

(25) Luo, Z.; Liu, H.; Spann, B. T.; Feng, Y.; Ye, P.; Chen, Y. P.; Xu, X. Measurement of In-Plane Thermal Conductivity of Ultrathin Films Using Micro-Raman Spectroscopy. *Nanoscale Microscale Thermophys. Eng.* **2014**, *18*, 183−193.

(26) Luo, Z.; Maassen, J.; Deng, Y.; Du, Y.; Garrelts, R. P.; Lundstrom, M. S.; Ye, P. D.; Xu, X. Anisotropic in-Plane Thermal Conductivity Observed in Few-Layer Black Phosphorus. *Nat. Commun.* **2015**, *6*, 8572.

(27) Cao, H.; Liu, C.; Tian, J.; Xu, Y.; Miotkowski, I.; Hasan, M. Z.; Chen, Y. P. Controlling and Distinguishing Electronic Transport of Topological and Trivial Surface States in a Topological Insulator. *arXiv:1409.3217*.

(28) Pan, Z. H.; Fedorov, A. V.; Gardner, D.; Lee, Y. S.; Chu, S.; Valla, T. Measurement of an Exceptionally Weak Electron-Phonon Coupling on the Surface of the Topological Insulator Bi_2Se_3 Using Angle-Resolved Photoemission Spectroscopy. *Phys. Rev. Lett.* **2012**, *108*, 187001.

(29) Zhu, X.; Santos, L.; Sankar, R.; Chikara, S.; Howard, C.; Chou, F. C.; Chamon, C.; El-Batanouny, M. Interaction of Phonons and Dirac Fermions on the Surface of Bi_2Se_3: A Strong Kohn Anomaly. *Phys. Rev. Lett.* **2011**, *107*, 186102.

(30) Qiu, B.; Sun, L.; Ruan, X. Lattice Thermal Conductivity Reduction in Bi_2Te_3 Quantum Wires with Smooth and Rough Surfaces: A Molecular Dynamics Study. *Phys. Rev. B: Condens. Matter Mater. Phys.* **2011**, *83*, 35312.

(31) Chang, J.; Jadaun, P.; Register, L. F.; Banerjee, S. K.; Sahu, B. Dielectric Capping Effects on Binary and Ternary Topological Insulator Surface States. *Phys. Rev. B: Condens. Matter Mater. Phys.* **2011**, *84*, 155105.

(32) Jenkins, G. S.; Schmadel, D. C.; Sushkov, A. B.; Drew, H. D.; Bichler, M.; Koblmueller, G.; Brahlek, M.; Bansal, N.; Oh, S. Dirac Cone Shift of a Passivated Topological Bi2Se3 Interface State. *Phys. Rev. B: Condens. Matter Mater. Phys.* **2013**, *87*, 155126.

(33) Goldsmid, H. J. *Introduction to Thermoelectricity*; Springer, 2010.

(34) Weathers, A.; Khan, Z. U.; Brooke, R.; Evans, D.; Pettes, M. T.; Andreasen, J. W.; Crispin, X.; Shi, L. Significant Electronic Thermal Transport in the Conducting Polymer poly(3,4-Ethylenedioxythiophene). *Adv. Mater.* **2015**, *27*, 2101−2106.

(35) Yoshino, H.; Murata, K. Significant Enhancement of Electronic Thermal Conductivity of Two-Dimensional Zero-Gap Systems by Bipolar-Diffusion Effect. *J. Phys. Soc. Jpn.* **2015**, *84*, 24601.

(36) Takeuchi, T. Thermal Conductivity of the Al-Based Quasicrystals and Approximants. *Z. Kristallogr. - Cryst. Mater.* **2009**, *224*, 35−38.

(37) Rhyee, J. S.; Cho, E.; Ahn, K.; Lee, K. H.; Lee, S. M. Thermoelectric Properties of Bipolar Diffusion Effect on $In_4Se_{3-x}Te_x$ Compounds. *Appl. Phys. Lett.* **2010**, *97*, 152104.

(38) Huang, B.-L.; Kaviany, M. Ab Initio and Molecular Dynamics Predictions for Electron and Phonon Transport in Bismuth Telluride. *Phys. Rev. B: Condens. Matter Mater. Phys.* **2008**, *77*, 125209.

(39) Chaput, L.; Pécheur, P.; Tobola, J.; Scherrer, H. Transport in Doped Skutterudites: Ab Initio Electronic Structure Calculations. *Phys. Rev. B: Condens. Matter Mater. Phys.* **2005**, *72*, 85126.

(40) Crossno, J.; Shi, J. K.; Wang, K.; Liu, X.; Harzheim, A.; Lucas, A.; Sachdev, S.; Kim, P.; Taniguchi, T.; Watanabe, K.; Ohki, T. A.; Fong, K. C. Observation of the Dirac Fluid and the Breakdown of the Wiedemann-Franz Law in Graphene. *Science* **2016**, *351*, 1058.

(41) Principi, A.; Vignale, G. Violation of the Wiedemann-Franz Law in Hydrodynamic Electron Liquids. *Phys. Rev. Lett.* **2015**, *115*, 56603.

(42) Lee, S.; Hippalgaonkar, K.; Yang, F.; Hong, J.; Ko, C.; Suh, J.; Liu, K.; Wang, K.; Urban, J. J.; Zhang, X.; Dames, C.; Hartnoll, S. A.; Delaire, O.; Wu, J. Anomalously Low Electronic Thermal Conductivity in Metallic Vanadium Dioxide. *Science* **2017**, *355*, 371−374.

(43) Foster, M. S.; Aleiner, I. L. Slow Imbalance Relaxation and Thermoelectric Transport in Graphene. *Phys. Rev. B: Condens. Matter Mater. Phys.* **2009**, *79*, 85415.

(44) Müller, M.; Fritz, L.; Sachdev, S. Quantum-Critical Relativistic Magnetotransport in Graphene. *Phys. Rev. B: Condens. Matter Mater. Phys.* **2008**, *78*, 115406.

(45) Kayyalha, M.; Maassen, J.; Lundstrom, M.; Shi, L.; Chen, Y. P. Gate-Tunable and Thickness-Dependent Electronic and Thermoelectric Transport in Few-Layer MoS2. *J. Appl. Phys.* **2016**, *120*, 134305.

(46) Jeong, C.; Kim, R.; Luisier, M.; Datta, S.; Lundstrom, M. On Landauer *versus* Boltzmann and Full Band *versus* Effective Mass Evaluation of Thermoelectric Transport Coefficients. *J. Appl. Phys.* **2010**, *107*, 23707.